Supporting Information

Ultrasensitive Room-Temperature H_2S Sensing Enabled by Interfacial Engineering via Bi-Shared Bi_2S_3/BiOI Heterostructures

Zhenze Zhou[a], Dianpeng Qi[a]*, Hui Zhang[b], Ming Zhu[c]*, Dan Shi[d], Meiling Yu[c], Haoxin Lei[c], Juanyuan Hao[c]*

[a] *School of Chemistry and Chemical Engineering, Harbin Institute of Technology, Harbin 150001, China.*

[b] *School of Chemistry and Materials Science, Hubei Engineering University, Xiaogan,432000, China.*

[c] *School of Materials Science and Engineering, Harbin Institute of Technology, Harbin 150001, China.*

[d] *State Key Laboratory of Efficient and Clean Coal-fired Utility Boilers, Harbin Boiler Company Limited, Harbin 150046, China.*

* Corresponding authors.

E-mail addresses: jyhao@hit.edu.cn (Juanyuan Hao*), dpqi@hit.edu.cn (Dianpeng Qi*), zhumingmilly@163.com (Ming Zhu*), zhou1996_edu@126.com (Zhenze Zhou), zhanghuiwxf@163.com (Hui Zhang), 18545653786@163.com (Dan Shi), 23B909005@stu.hit.edu.cn (Meiling Yu), 24S009009@stu.hit.edu.cn (Haoxin Lei).

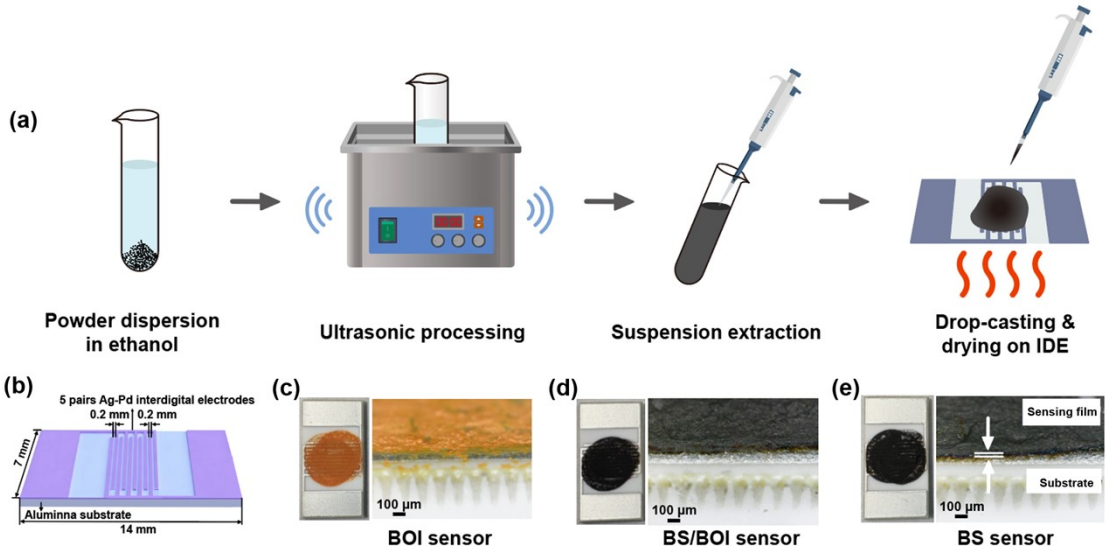

Fig. S1. (a) Schematic illustration of the sensor fabrication process. (b) Structural diagram and dimensions of the IDE substrate. (c–e) Optical images and corresponding cross-sectional views of the BOI, BS/BOI, and BS sensing films deposited on the IDE substrate.

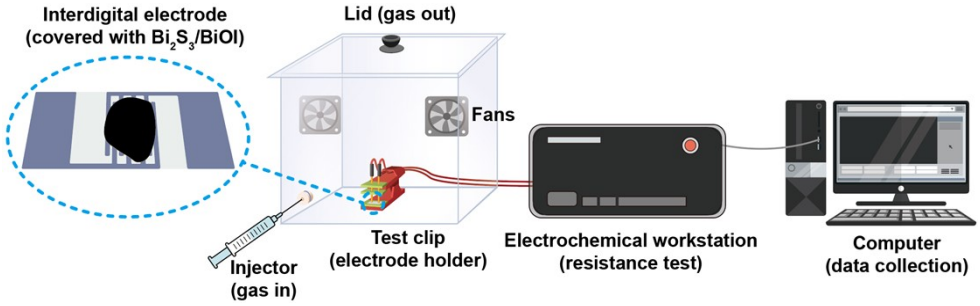

Fig. S2. Gas sensing test system schematic.

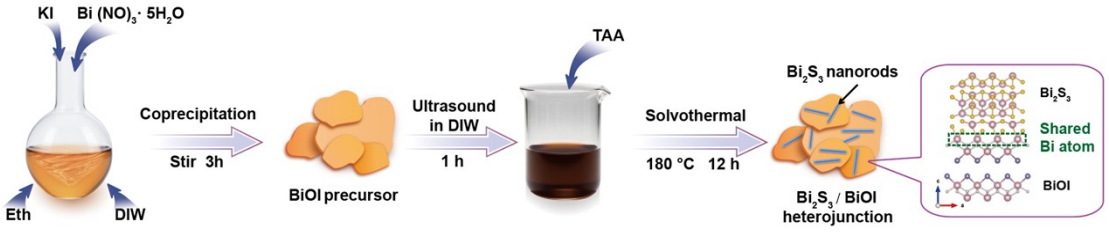

Fig. S3. Schematic illustration for the synthesis procedure of the Bi_2S_3/BiOI heterostructures.

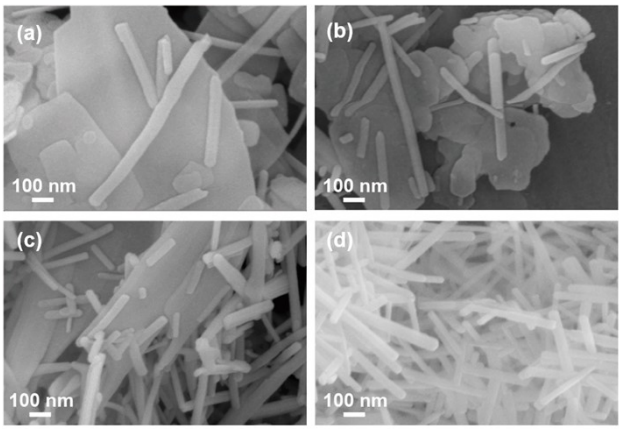

Fig. S4 SEM images of (a) BS/BOI-1, (b) BS/BOI-2, (c) BS/BOI-3 and (d) BS.

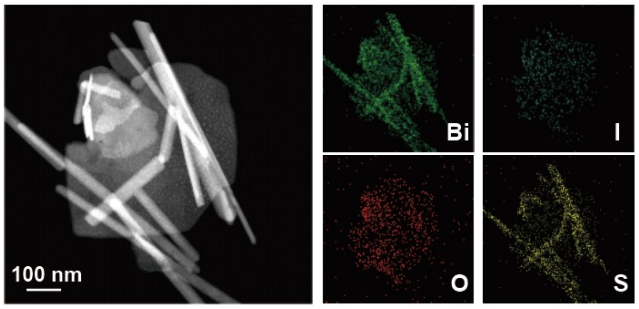

Fig. S5. EDX elemental mapping images of the Bi_2S_3/BiOI heterostructures.

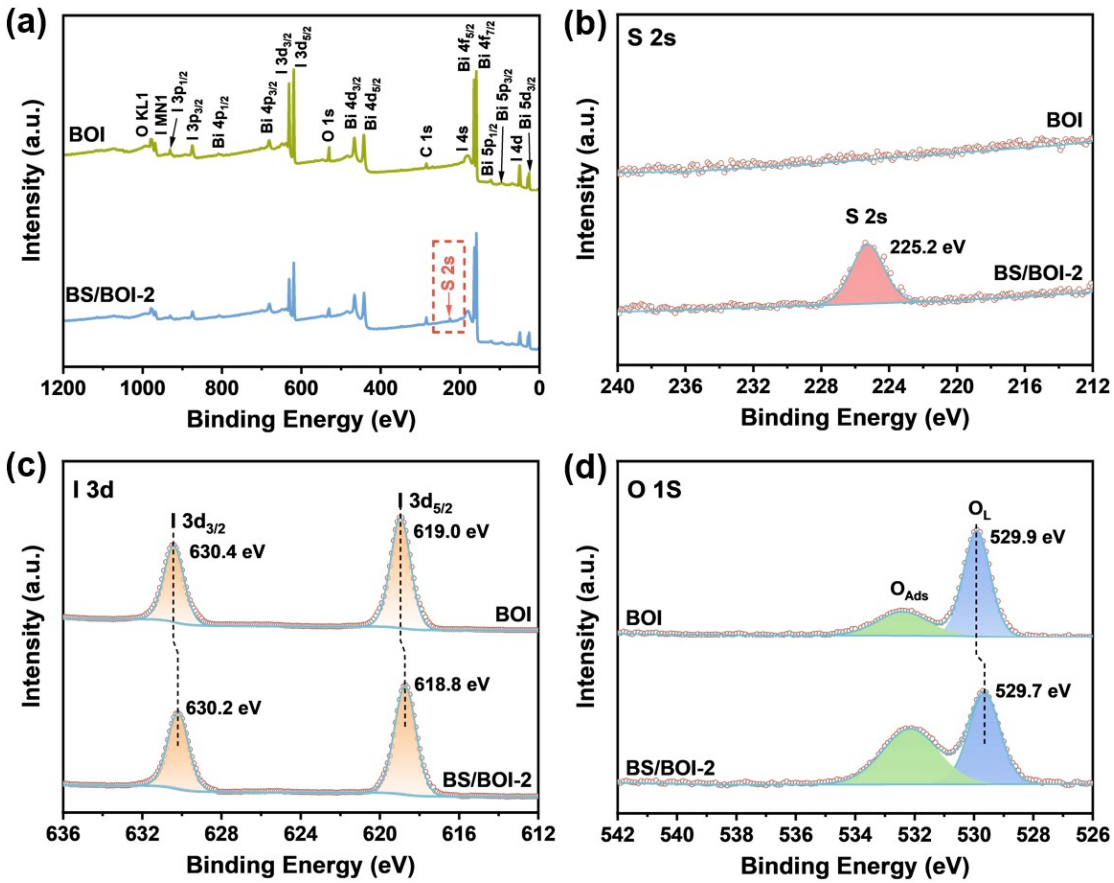

Fig. S6. XPS survey spectrum (a) and High-resolution XPS spectra of (b) S 2s, (c) I 3d, and (d) O 1s for BOI and BS/BOI-2.

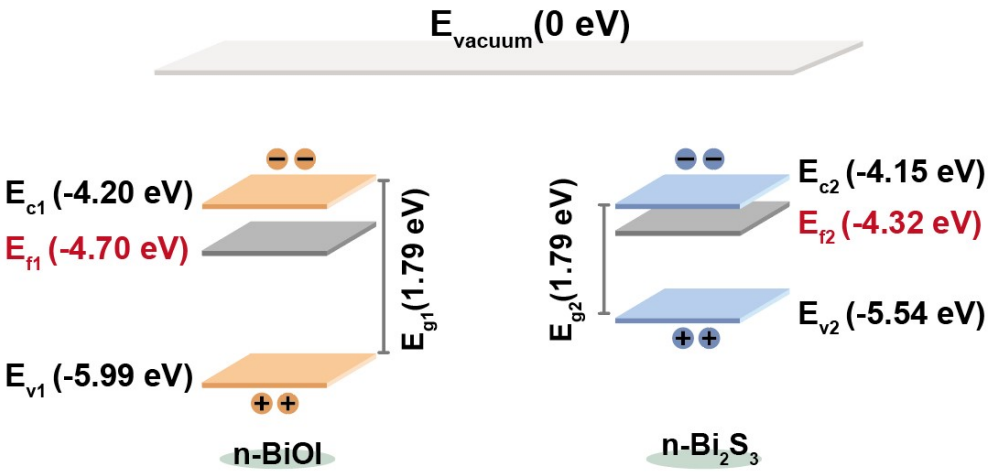

Fig. S7. Schematic band structures of BiOI and Bi_2S_3.

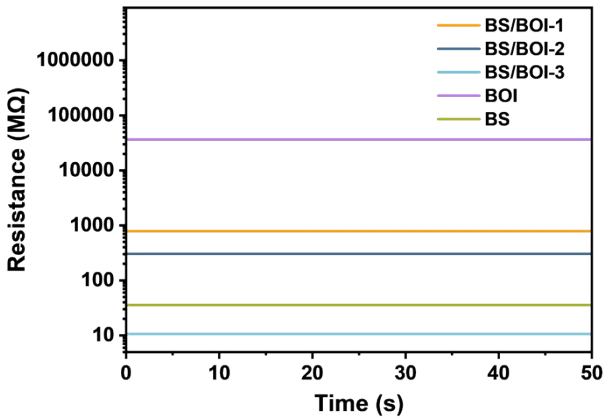

Fig. S8. Baseline resistance of BOI, BS/BOI-1, BS/BOI-2, BS/BOI-3 and BS sensors.

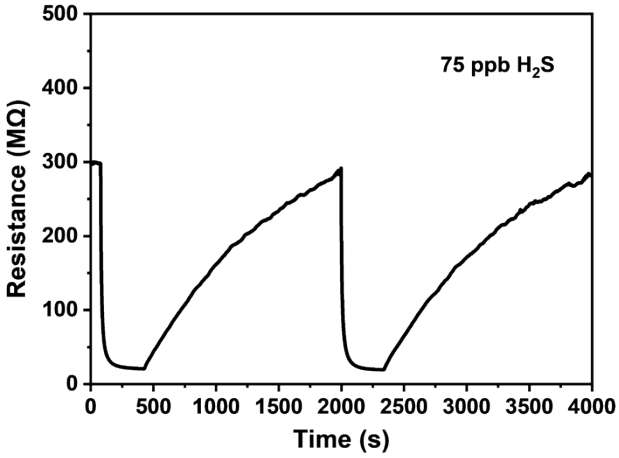

Fig. S9. Resistance test curves of the BS/BOI-2 sensor exposed to 75 ppb H_2S.

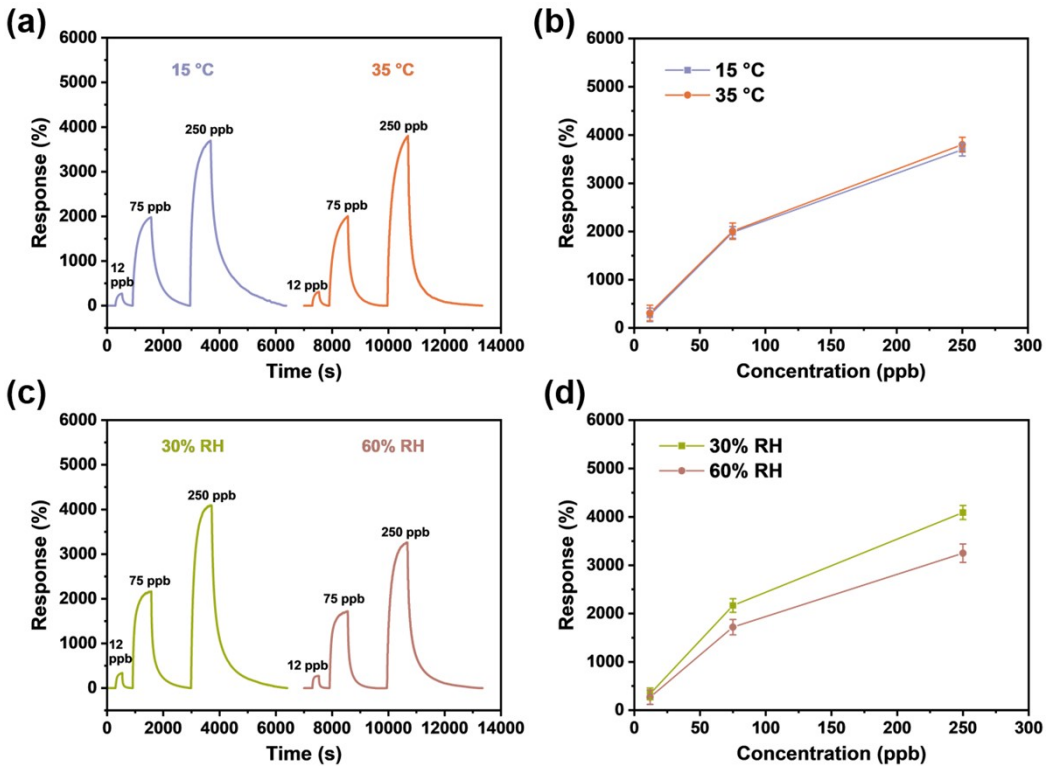

Fig. S10. Influence of temperature and humidity on the H_2S sensing performance. (a) Dynamic response curves at 15 and 35 °C. (b) Corresponding calibration curves under different temperature conditions. (c) Dynamic response curves at different H_2S concentrations under 30% RH and 60% RH. (d) Corresponding calibration curves under different humidity conditions.

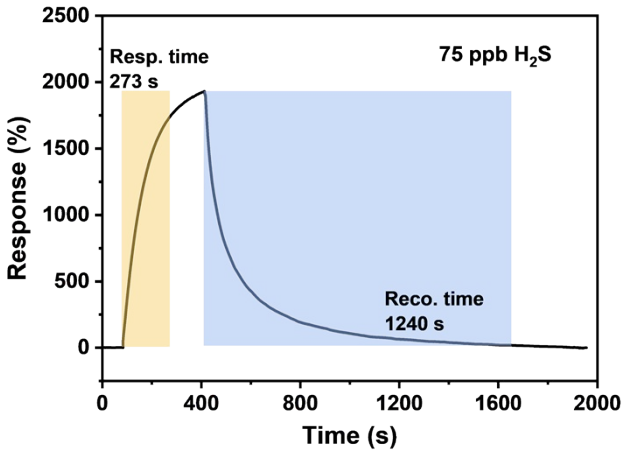

Fig. S11. Response/recovery times for the BS/BOI-2 sensor exposed to 75 ppb H_2S.

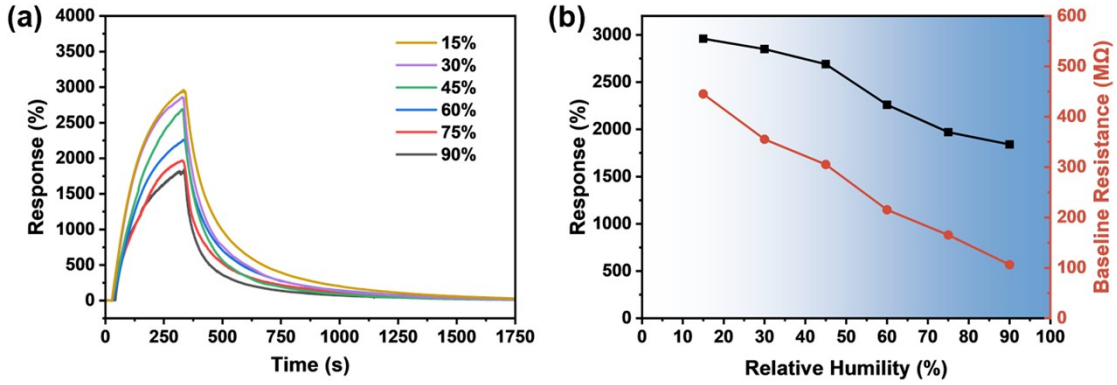

Fig. S12. (a) The response curves and (b) baseline resistance and sensing response of the BS/BOI-2 sensor to 125 ppb H_2S under different relative humidity conditions (15-90%).

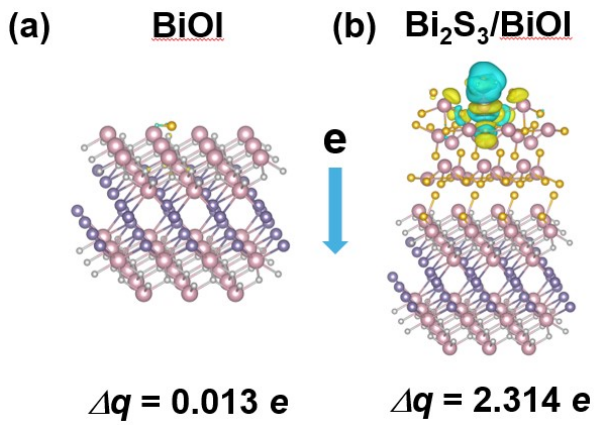

Fig. S13. Bader charge and differential charge density analysis of H_2S on pristine BiOI and the Bi_2S_3/BiOI heterostructure.

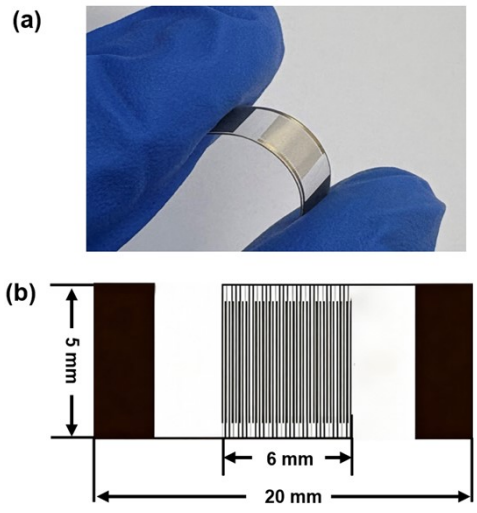

Fig. S14. Optical image (a) and schematic diagram (b) of the flexible electrode.

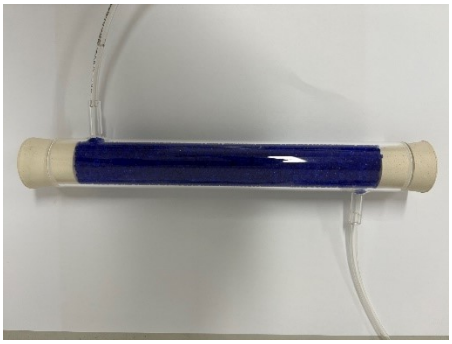

Fig. S15. Photographic image of the dehumidification apparatus.

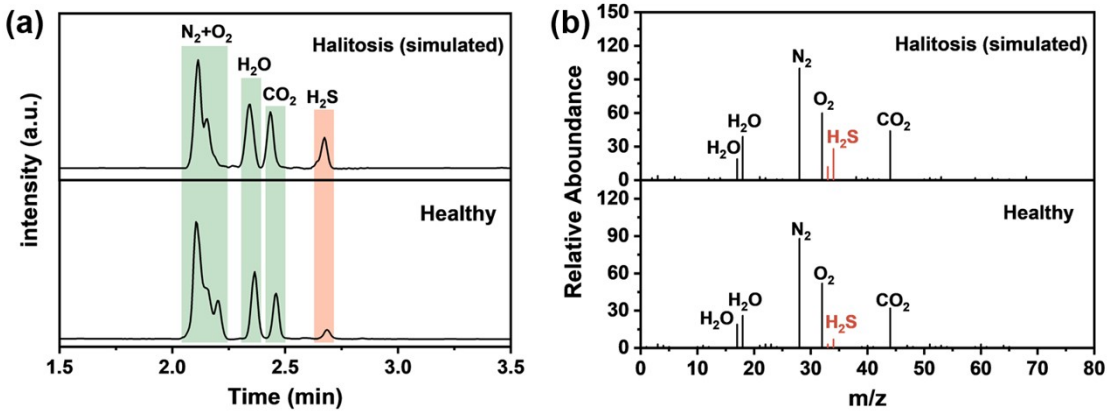

Fig. S16. GC chromatograms (a) and the corresponding mass spectra (b) of simulated halitosis breath and healthy breath samples.

Table S1. Hall effect measurement results of BiOI, BS/BOI-2, and Bi_2S_3

Sample	Type	Carrier concentration (cm^{-3})	Mobility ($cm^2V^{-1}s^{-1}$)	Conductivity ($S \cdot cm^{-1}$)
BiOI	n	4.91×10^{13}	0.08	6.28×10^{-7}
BS/BOI-2	n	2.42×10^{14}	0.62	2.40×10^{-5}
Bi_2S_3	n	1.79×10^{15}	1.38	3.95×10^{-4}

Supplementary Note 1: Calculation method for theoretical detection limit

The theoretical detection limit (TDL) was calculated using a signal-to-noise ratio > 3 as the sensing criterion. First, we collected ten data points from the baseline response before H_2S exposure. A fifth-order polynomial fitting was applied to determine the average response value, and the variance was calculated using equation (1), where y is the average response value and y_i is the collected response value.

$$R_{x^2} = \sum (y_i - y)^2 \quad (1)$$

Next, the root means square noise (RMS_{noise}) was calculated using equation (2), where N is the number of extracted data points.

$$RMS_{\text{noise}} = \sqrt{\frac{R_{x^2}}{N}} \quad (2)$$

Finally, the theoretical TDL was determined by using equation (3) and the slope value was obtained from the linear concentration-response relationship

$$\text{TDL} = 3\frac{RMS_{\text{noise}}}{\text{slope}} \quad (3)$$